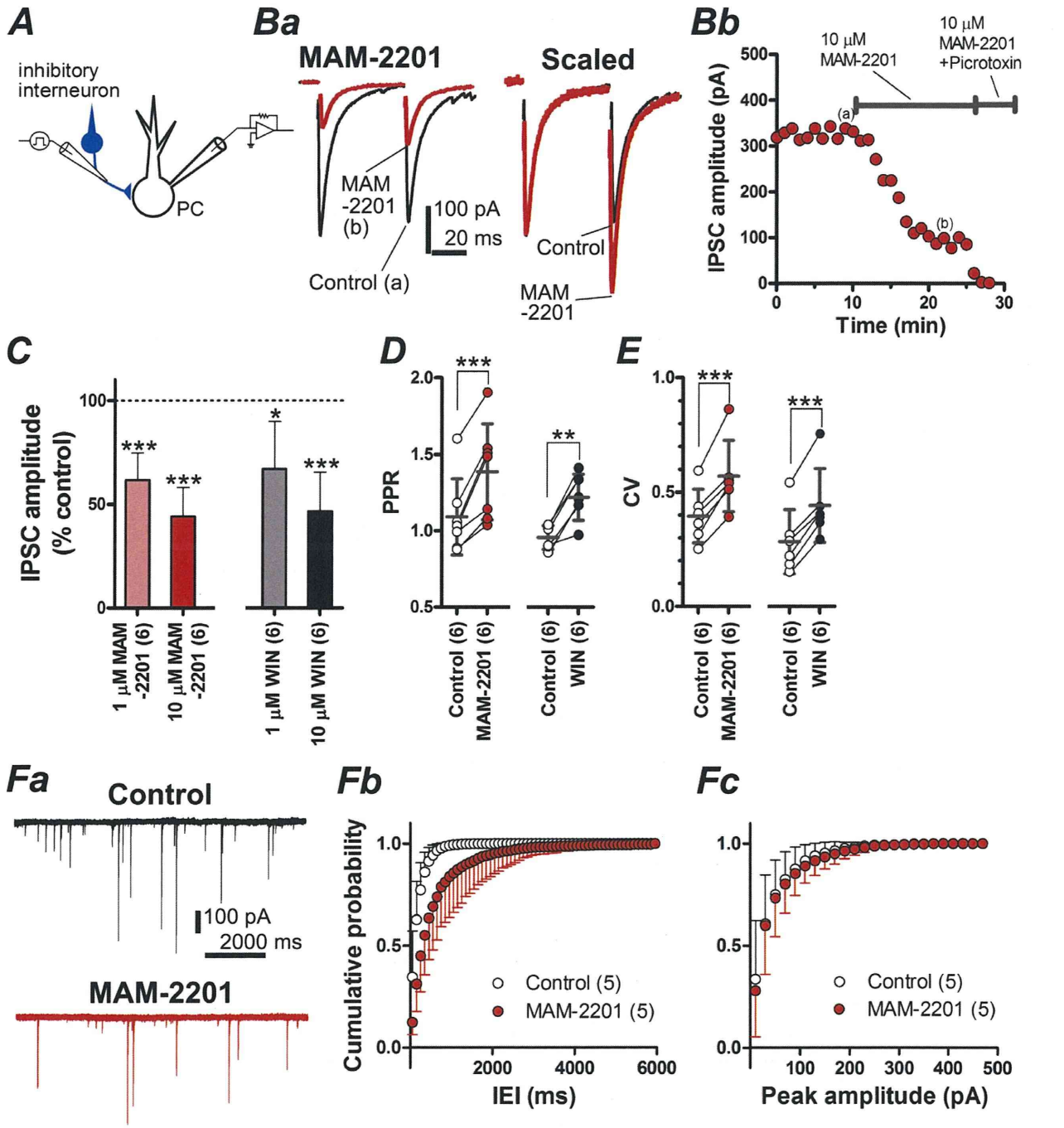

Fig. 5. MAM-2201 reduces GABAergic synaptic transmission at interneuron-PC synapses via presynaptic mechanisms. *A*, Experimental configuration for Fig. 5*B–E*. *Ba*, Averaged current traces of IPSCs in control conditions (Control) and 10 μM MAM-2201. These traces show normalized IPSC responses at time points marked (a) and (b) in *Bb*. IPSCs were evoked with pairs of stimuli (50 ms interval) in the presence of 40 μM DNQX and were recorded as inward currents because of the use of the CsCl-based internal solution. The holding potential was −80 mV, and stimulus artifacts were blanked for clarity. The first peak in MAM-2201 was reduced to 28.0% of control. In the right panel, the first IPSC in MAM-2201 is scaled to the amplitude of the first IPSC in Control (Scaled), showing a clear increase of PPR. *Bb*, Time course of peak amplitudes of the first IPSC. Each point represents an averaged value obtained from six consecutive records. *C*, Concentration-dependent decreases of peak amplitude of IPSC by MAM-2201 and WIN. IPSC amplitudes were normalized to the control value (=baseline responses) and expressed as a percentage of control. $*p < 0.05$ and $***p < 0.001$. *D* and *E*, Summary of PPR (*D*) and CV (*E*) of IPSCs before and after application of MAM-2201 and WIN (10 μM in both groups). $**p < 0.01$. *F*, Miniature IPSCs (mIPSCs) recorded in the presence of tetrodotoxin (TTX, 1 μM) and DNQX. *Fa*, Five superimposed traces before (Control) and after application of MAM-2201. mIPSCs appear as downward current deflections. *Fb* and *Fc*, Average cumulative probability histograms of IEI (*Fb*, bin width: 100 ms) and peak amplitude (*Fc*, bin width: 20 pA) of mIPSCs.

decreased PF-PC qEPSC frequency [Inter-event interval (IEI), Control: 194.0 ± 24.1 ms, MAM-2201: 288.7 ± 30.2 ms, $p < 0.001$, $n = 6$, Fig. 3*Fa* and *Fb*] without affecting PF-PC qEPSC amplitude (peak amplitude, Control: 18.9 ± 2.1 pA, MAM-2201: 18.6 ± 4.3 pA, $p = 0.860$, $n = 6$, Fig. 3*Fa* and *Fc*). In the absence of MAM-2201, amplitudes of PF-PC EPSCs did not show significant changes during 45-min recording under condition in which series resistance was stable (105.2 ± 10.5% of control, $n = 7$, $p = 0.271$).

Table 1
IC50s of synthetic cannabinoids against PF-PC EPSCs.

	WIN	MAM-2201	JWH-018
IC50 (μM) [95% CI (μM)][a]	0.890 [0.296-2.679]	0.363 [0.193-0.681]	1.121 [0.551-2.282]
Relative IC50	1.00	0.41	1.25

[a] Data are provided as the best-fit values with 95% confidence intervals (CI).

To examine whether MAM-2201 altered postsynaptic responses by activating presynaptic CB1Rs, MAM-2201 was bath-applied to the cerebellar slices in the presence of AM251 (5 μM). MAM-2201 did not induce any change of PF-PC EPSC amplitude in the presence of AM251 (Fig. 3G, 102.2 ± 6.0% of control, $n = 5$, $p = 0.443$). Subsequent application of DNQX (40 μM) abolished PF-PC EPSCs, demonstrating that glutamatergic synaptic transmission was indeed evoked, and bath application of these chemicals was successful (Fig. 3Ga). Taken together, these results indicate that the MAM-2201-induced changes are mediated by a decrease in presynaptic neurotransmitter release from PF terminals via activation of presynaptic CB1Rs.

3.3. MAM-2201 is a more potent inhibitor of PF-PC synapses than Δ^9-THC and JWH-018

Fig. 4A–C show representative traces of PF-PC EPSCs in the presence of MAM-2201 (Fig. 4A), JWH-018 (Fig. 4B), or Δ^9-THC (Fig. 4C), respectively. The inhibitory effect of MAM-2201 on PF-PC

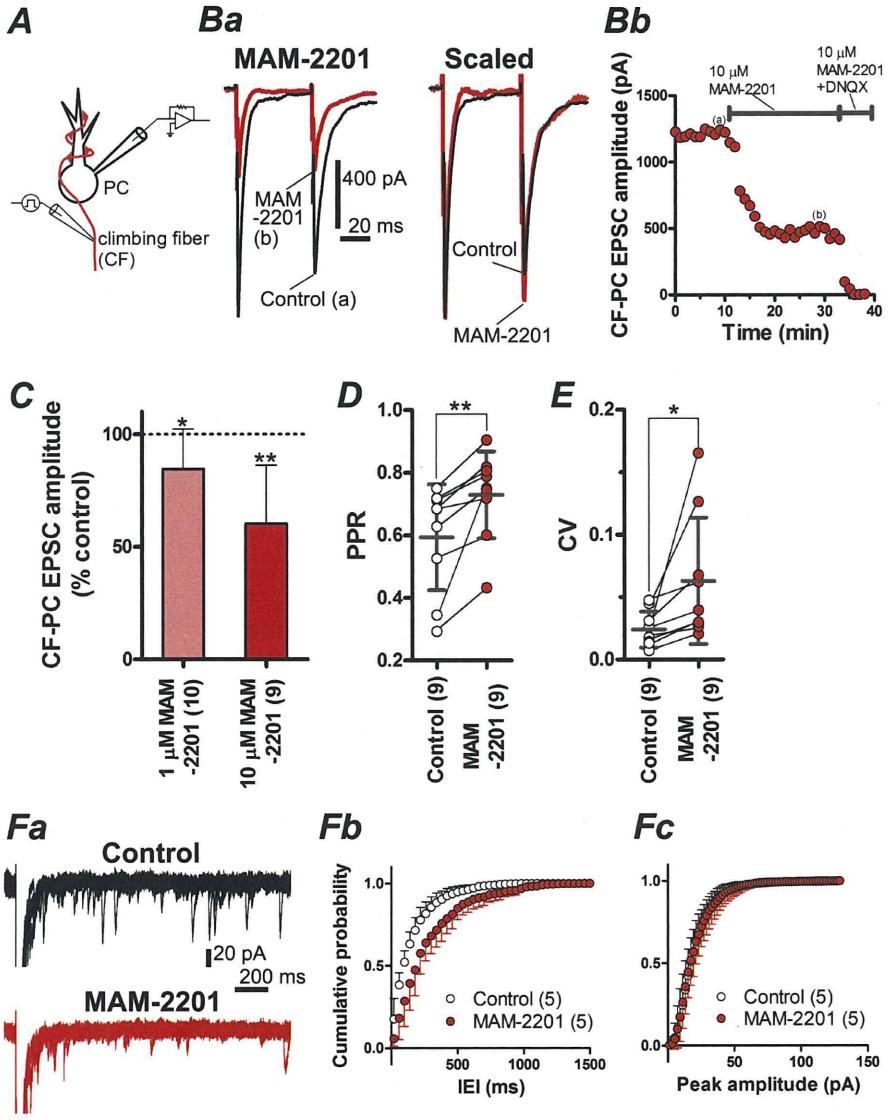

Fig. 6. MAM-2201-mediated presynaptic inhibition at climbing fiber (CF)-PC synapses. *A*, Experimental configuration for Fig. 6*B–F* and 7. *Ba*, Averaged current traces of CF-PC EPSCs in control (Control) and 10 μM MAM-2201. These traces show normalized CF-PC EPSC responses at time points marked (a) and (b) in *Bb*. CF-PC EPSCs were evoked with pairs of stimuli (50 ms interval) in the presence of 100 μM picrotoxin. PCs were held at −10 mV to reduce the driving force for AMPA receptor-mediated currents. Stimulus artifacts were truncated for clarity. The first peak in MAM-2201 was reduced to 38.4% of control. In the right panel, the first CF-PC EPSC in MAM-2201 is scaled to the amplitude of the first CF-PC EPSC of control (Scaled). *Bb*, Time course of peak amplitudes of first CF-PC EPSC. Each point represents an averaged value obtained from six consecutive records. *C*, Concentration-dependent decreases of the peak amplitudes of CF-PC EPSCs by MAM-2201. CF-PC EPSC amplitudes were expressed as a percentage of control. $*p < 0.05$ and $**p < 0.001$. *D* and *E*, Summary of PPR (*D*) and CV (*E*) of CF-PC EPSCs before and after application of MAM-2201 (10 μM). *F*, CF-PC qEPSCs in the presence of picrotoxin and Sr^{2+} (2 mM $SrCl_2$). The qEPSCs were recorded at a holding potential of −80 mV. *Fa*, Five superimposed traces before (Control) and after application of MAM-2201. Synchronous CF-PC EPSCs are truncated. *Fb* and *Fc*, Average cumulative probability histograms of IEI (*Fb*, bin width: 40 ms) and peak amplitude (*Fc*, bin width: 2 pA) of CF-PC qEPSCs.

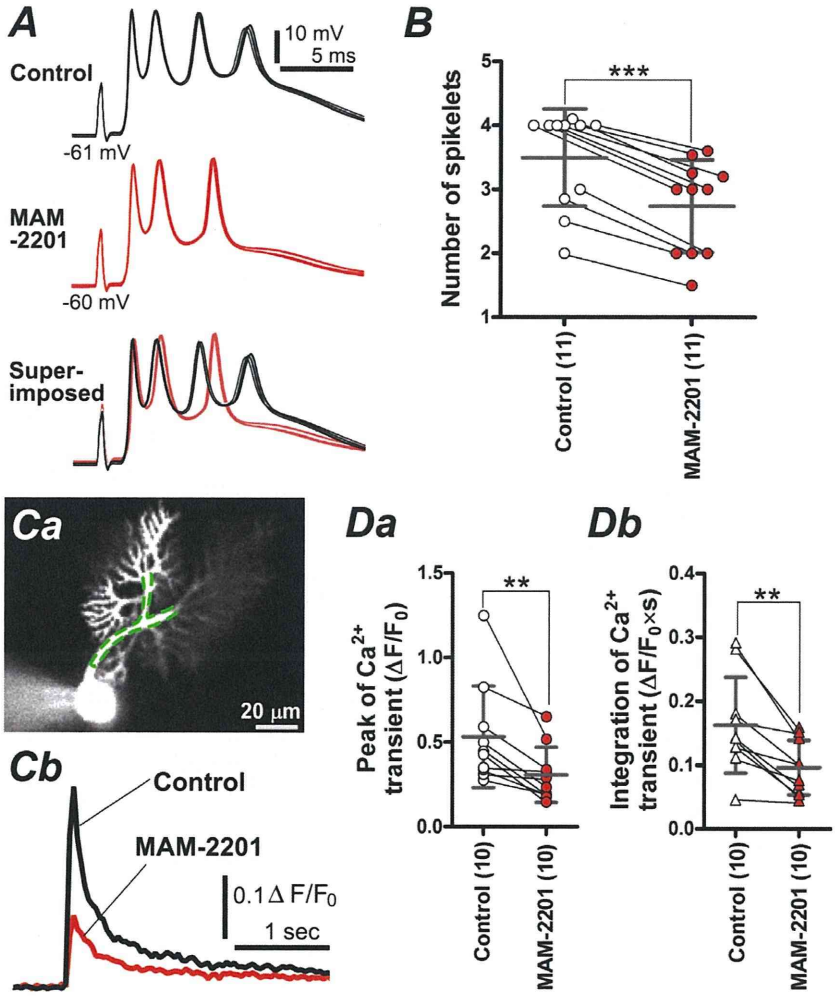

Fig. 7. MAM-2201 reduces the number of spikelets in complex spikes and dendritic Ca^{2+} transients evoked by CF stimulation. *A–D*, Simultaneous recordings of complex spikes and dendritic Ca^{2+} transients. *A*, Representative superimposed traces of complex spikes (5 traces) evoked by stimulation of CFs (0.1 Hz) in the presence of picrotoxin at near physiological temperature (34 ± 1 °C). The K-gluconate-based intracellular solution containing Oregon Green 488 BAPTA-1 hexapotassium salt (OGB-1, 100 μM) was used for current-clamp recordings. At the start of the recording, the resting membrane potential was adjusted around −60 to −70 mV by current injection to prevent spontaneous firing. MAM-2201 (10 μM, 10 min) reduced the number of spikelets (4 spikelets in Control; 3 spikelets in MAM-2201). Superimposed traces reveal delay and reduction of spikelets in MAM-2201. *B*, Summary of average number of spikelets before and after application of MAM-2201 (10 μM). ***$p < 0.001$. *C*, A dendritic Ca^{2+} transient induced by CF stimulation. Intracellular Ca^{2+} measurement in *C* was simultaneously performed while recording the complex spikes in *A*. *Ca*, Representative confocal image of PC loaded with OGB-1 via a patch pipette. Area indicated by dotted line represents region of interest used for the calculation of the dendritic Ca^{2+} transients. *Cb*, Representative Ca^{2+} transients in control and MAM-2201 (10 μM). F_0 is the fluorescence intensity when the cells were at rest, and ΔF is the absolute values of fluorescence changes during activity. *Da* and *Db*, Summary of Ca^{2+} transient peaks (*Da*) and integration of Ca^{2+} transients (*Db*). The integration was performed for 2 s from the onset. **$p < 0.01$.

EPSC amplitude was first detectable at 0.03 μM (Fig. 4*D*, 90.1 ± 6.1% of control, $n = 5$, $p < 0.05$), and became more apparent at higher concentrations. Application of 0.1 μM MAM-2201 was sufficient to induce a clear reduction [trace (b) in Fig. 4*Aa*, 71.9% of control], and subsequent administration of 1 μM MAM-2201 induced further decrease [trace (c) in Fig. 4*Aa*, 51.0% of control]. On the other hand, 0.1 μM JWH-018 did not have detectable effects on PF-PC EPSCs [trace (b) in Fig. 4*Ba*, 99.0% of control; 0.1 μM JWH-018 in Fig. 4*D*, $n = 7$, $p = 0.096$]. Higher concentrations of JWH-018 were required to reduce PF-PC EPSC amplitude [trace (c) in Fig. 4*Ba*, 1 μM, 81.0% of control; trace (d) in Fig. 4*Ba*, 30 μM, 44.2% of control]. Application of Δ^9-THC, which acts as a partial agonist of CB1Rs (Shen and Thayer, 1999; Luk et al., 2004), decreased amplitude of PF-EPSCs obviously at 3 μM [trace (b) in Fig. 4*C*, 68.6% of control], but subsequent administration of 30 μM Δ^9-THC did not induce a clear reduction [trace (c) in Fig. 4*C*, 57.0% of control]. Δ^9-THC (30 μM) significantly increased PPR and CV ($n = 6$, data not shown), indicating a decrease in presynaptic neurotransmitter release. Fig. 4*D* shows the concentration-dependent decreases of PF-PC EPSC amplitude induced by cannabinoid-related compounds. MAM-2201 decreased PF-PC EPSCs more potently than JWH-018 within the range of 0.03–3 μM (Fig. 4*D*, blue triangles (in the web version), $p < 0.05$ and $p < 0.01$ by unpaired *t*-tests test) and Δ^9-THC within the range of 0.1–30 μM (Fig. 4*D*, gray squares, $p < 0.001$ by unpaired *t*-tests test). Application of WIN decreased PF-PC EPSC amplitude to 64.5 ± 0.16% ($n = 7$) of the control value at a concentration of 1 μM and to 46.8 ± 0.13% ($n = 12$) at 10 μM (Fig. 4*D*, WIN). These results are comparable to the previous reports using cerebellar slice preparations from rodents (see Discussion) (Levenes et al., 1998; Takahashi and Linden, 2000; Kawamura et al., 2006). The IC50s of the synthetic cannabinoids against PF-PC EPSCs are summarized in Table 1, and indicate that the rank order of potency for inhibition is MAM-

Table 2
MAM-2201 did not affect intrinsic membrane properties of PCs.

	Control ($n = 10$)	10 μM MAM-2201 ($n = 10$)	p value
Resting membrane potential (mV)	−65.3 ± 3.2	−66.0 ± 3.5	0.43
input resistance (MΩ)	113 ± 51	101 ± 34	0.29
Threshold current (pA)	71.0 ± 39.5	77.8 ± 7.4	0.24
Threshold potential (mV)	−45.4 ± 5.6	−44.9 ± 6.4	0.50
Spike height (mV)	44.9 ± 6.4	45.4 ± 47.6	0.71
Maximum rate of rise (V/s)	114 ± 40	131 ± 37	0.20
Maximum rate of fall (V/s)	−93.0 ± 17	−89.2 ± 15.8	0.14
Firing frequency at 200 pA (Hz)	33.0 ± 18.4	34.4 ± 20.5	0.77
Firing frequency at 500 pA (Hz)	72.6 ± 29.8	77.8 ± 42.1	0.68

Young mice (P14–20) and the K-gluconate-based internal solution were used for the experiments. Current-clamp recordings were performed at near physiological temperature (34 ± 1 °C).
Data are provided as the means ± standard deviation, and n = number of experiments.

2201 > WIN > JWH-018. These findings are consistent with our unpublished data on the IC50s for these synthetic cannabinoids, measured by a binding assay for human recombinant CB1Rs (see Discussion). IC50 of Δ^9-THC was not able to be calculated due to ambiguous fitting. These results demonstrate that MAM-2201 is a more potent inhibitor of PF-PC synaptic transmission than JWH-018 and Δ^9-THC.

3.4. MAM-2201 inhibits GABAergic synaptic transmission at inhibitory interneuron-PC synapses via presynaptic mechanisms

PCs receive feed-forward inhibition from GABAergic inhibitory interneurons lying in the molecular layer of the cerebellar cortex (Llinas et al., 2004), and this inhibition shapes the spike output of PCs (Mittmann et al., 2005). To explore how MAM-2201 modulates this inhibitory synaptic input, we recorded GABAergic synaptic transmission at inhibitory interneuron-PC synapses and examined the effects of MAM-2201 on inhibitory transmission. As shown in Fig. 5*B*, 10 μM MAM-2201 decreased the first IPSC amplitude (MAM-2201 in Fig. 5*Ba* and *Bb*; Fig. 5*C*, $n = 6$, $p < 0.001$), and a similar reduction was observed by 1 μM MAM-2201, indicating the MAM-2201-induced decrease was concentration-dependent (Fig. 5*C*, MAM-2201). MAM-2201 (10 μM) significantly increased PPR and CV (Scaled in Fig. 5*Ba*, *D* and *E*, MAM-2201), and these increases were comparable to those obtained by WIN (10 μM, Fig. 5*D* and *E*, WIN). Moreover, MAM-2201 (10 μM) decreased mIPSC frequency (IEI, Control: 451.2 ± 464.1 ms, MAM-2201: 718.8 ± 542.9 ms, $p < 0.05$, $n = 5$, Fig. 5*Fa* and *Fb*) without affecting mIPSC amplitude (peak amplitude, Control: 45.3 ± 22.3 pA, MAM-2201: 48.3 ± 24.1 pA, $p = 0.53$, $n = 5$, Fig. 5*Fa* and *Fc*). These results demonstrate that MAM-2201 inhibits GABAergic synaptic transmission at interneuron-PC synapses via presynaptic mechanisms.

3.5. MAM-2201-mediated presynaptic inhibition at CF-PC synapses reduces the number of spikelets in complex spikes and dendritic Ca^{2+} transients in PCs

Activation of CFs produces AMPA receptor-mediated strong postsynaptic depolarization and evokes an all-or-none spike with multiple peaks (spikelets), called "complex spikes" in the soma (Llinas et al., 2004). Complex spikes are accompanied by a large, dendritic Ca^{2+} transient, which plays a crucial role in producing long-term depression (LTD) at PF-PC synapses (Konnerth et al., 1992). At CF terminals, activation of presynaptic CB1Rs by WIN reduces glutamate release (Maejima et al., 2001). To examine how presynaptic modulation by MAM-2201 at CF-PC synapses affects the waveforms of complex spikes and CF-induced dendritic Ca^{2+} transients, we first confirmed presynaptic inhibition by MAM-2201 at CF-PC synapses (Fig. 6), and then performed simultaneous recordings of complex spikes and intracellular Ca^{2+} transients (Fig. 7).

First, CF-PC EPSCs were recorded at the holding potential of −10 mV in the presence of picrotoxin (Fig. 6*B–E*). To improve the space clamp in dendrites, young mice (P14–20) were used for the following experiments. This was because CF innervation of PCs is almost matured at this age (Hashimoto and Kano, 2013), and their dendrites are compact compared with those of adult (~P57) mice (McKay and Turner, 2005). As shown in Fig. 6*B* and *C*, bath application of MAM-2201 (1 or 10 μM) reduced CF-PC EPSC amplitude in a concentration-dependent manner. This reduction was accompanied by significant increases in PPR and CV (10 μM MAM-2201; Scaled in Fig. 6*Ba*, *C* and *D*). Moreover, MAM-2201 (10 μM) decreased CF-PC qEPSC frequency (IEI, Control: 176.5 ± 40.3 ms, MAM-2201: 234.5 ± 51.1 ms, $p < 0.01$, $n = 5$, Fig. 6*Fa* and *Fb*) without affecting CF-PC qEPSC amplitude (peak amplitude, Control: 22.5 ± 2.7 pA, MAM-2201: 22.0 ± 4.0 pA, $p = 0.75$, $n = 5$, Fig. 6*Fa* and *Fc*). These results indicate that MAM-2201 presynaptically inhibits neurotransmitter release from CF terminals.

We then simultaneously recorded complex spikes in the somata and Ca^{2+} transients in the dendrites of PCs using the K-gluconate-based internal solution containing OGB-1 at near physiological temperature. Complex spikes were elicited under current-clamp conditions. As presented in Fig. 7*A*, electrical stimulation of CFs evoked all-or-none complex spikes consisting of spikelets (Control in Fig. 7*A*). MAM-2201 (10 μM, 10 min) significantly reduced the number of spikelets to 78% of the control (Fig. 7*B*, $n = 11$, $p < 0.001$). Because MAM-2201 modulated synaptic properties via activation of presynaptic CB1Rs (Fig. 3), and because PCs do not express CB1Rs (Kano et al., 2009), we would not expect MAM-2201 to affect the intrinsic membrane properties of PCs. As expected, we were able to confirm that MAM-2201 did not affect the resting membrane potential, input resistance, or action potential properties of PCs (Table 2). Accordingly, MAM-2201-induced changes in complex spike waveforms can be interpreted based on depression of CF-PC EPSCs. The complex spikes evoked by CF stimulation were accompanied by large Ca^{2+} transients in the dendrites (Fig. 7*Cb*, Control). MAM-2201 substantially decreased the peak amplitude of the Ca^{2+} transient (Fig. 7*Cb*, MAM-2201). Both the peak and the integral of the Ca^{2+} transients were significantly attenuated by 10 μM MAM-2201 (peak: $n = 10$, $p < 0.01$, Fig. 7*Da*; integration: $n = 10$, $p < 0.01$, Fig. 7*Db*). Taken together, these results indicate that MAM-2201 alters PC responses to CF activation by reducing the number of spikelets and the dendritic Ca^{2+} transients. This implies that MAM-2201 would decrease complex spike-mediated information propagation from PCs to the next nuclei and might affect induction of intracellular Ca^{2+}-dependent LTD at PF-PC synapses (see Discussion).

4. Discussion

This is the first study of the effects of MAM-2201 on neuronal functions. We found that MAM-2201 acted as an agonist of CB1Rs (Fig. 2). We also found that MAM-2201 inhibited glutamatergic synaptic transmission presynaptically via activation of presynaptic CB1Rs (Fig. 3). At the same concentrations, MAM-2201 decreased PF-PC EPSCs more potently than JWH-018 and Δ^9-THC (Fig. 4). Moreover, MAM-2201 also presynaptically suppressed GABAergic synaptic transmission at interneuron-PC synapses (Fig. 5) and glutamatergic synaptic transmission at CF-PC synapses (Fig. 6). In the case of smaller CF-PC EPSCs, MAM-2201 led to reduction of the number of action potentials in complex spikes and to reduced

dendritic intracellular Ca^{2+} transients (Fig. 7). Thus, it is likely that, in humans, the psychoactive effects caused by MAM-2201 are mainly due to inhibition of neurotransmitter release via activation of presynaptic CB1Rs.

4.1. The validity of our data on presynaptic inhibition at PF-PC synapses induced by synthetic cannabinoids

In our experiments, WIN reduced PF-PC EPSC amplitude to 64.5% (1 μM) and 46.8% (10 μM) of the control value using P20–57 mice (Fig. 4*D*). These reductions are comparable to previously published values obtained from acute cerebellar slice preparations: 55.6% of control in 1 μM WIN (P15–21 rats) (Levenes et al., 1998), 29.1 and 12.3% in 1 and 5 μM WIN, respectively (P15–19 rats) (Takahashi and Linden, 2000), and 23.5% in 5 μM WIN (P9–14 mice) (Kawamura et al., 2006). The latter two reports show somewhat smaller percentages compared with our data, but this can be attributed to the differences in the ages of the animals used: an immunohistochemical study revealed that the distribution patterns of CB1Rs in the molecular layer show developmental changes (Kawamura et al., 2006).

Atwood et al. reported that the IC50 of JWH-018 against synaptic transmission is 14.9 nM using autaptic hippocampal neuronal cultures (Atwood et al., 2010), whereas our IC50 value for JWH-018 was approximately 100 times larger than that of their report (Table 1). This discrepancy might be explained by the different neuronal preparations used: Atwood et al. utilized dissociated neuronal cultures, whose synapses would not be wrapped by cell structures such as glial membranes. These synapses would be more easily exposed to CB1R agonists compared with those in cerebellar slice preparations, and therefore synaptic transmission in the autaptic hippocampal cultures might be suppressed by a lower concentration of JWH-018.

Using a binding assay for human recombinant CB1Rs, we recently found that relative IC50s for WIN, MAM-2201, and JWH-018 against CB1Rs were 1.00, 0.70, and 5.30, respectively (Kikura-Hanajiri et al., manuscript in preparation). These data agree well with our observation of the relative IC50s against excitatory neurotransmitter release from PF terminals to PCs using cerebellar slice preparations (Table 1). Therefore, we consider our observations of IC50s in cerebellar preparations to be reasonable.

4.2. Adverse effects of MAM-2201 on targets of the cerebellar cortex and on cerebellum-dependent motor functions

PCs are the sole output GABAergic neurons from the cerebellar cortex and make direct synaptic contacts onto the deep cerebellar nuclear neurons and vestibular nuclear neurons (Voogd and Glickstein, 1998; Zheng and Raman, 2010). PCs receive two types of excitatory input from CFs and PFs. CFs arise from the inferior olivary complex located in the brainstem. CFs are activated during motor learning and induce complex spikes in PCs (Ito, 2001; Llinas et al., 2004). Spikelets in complex spike can propagate to the synaptic terminals of PCs (Khaliq and Raman, 2005). PFs are the axons of granule cells, which are excited by glutamatergic mossy fiber inputs. Mossy fibers originate from nuclei in the spinal cord and brain stem. The mossy fiber-PF pathway is the main operational input to the cerebellum and PCs, and carries afferent information both from the periphery and from other brain centers. PFs produce a brief excitatory postsynaptic potential in PCs that generates a single action potential called a "simple spike." In addition, PCs receive feed-forward synaptic inhibition from GABAergic interneurons, and this inhibition increases the precision of PC spike outputs (Mittmann et al., 2005). Thus, all of these synaptic inputs to PCs can control the output of the cerebellar cortex. The absence of PC activity or genetic manipulation of synaptic transmission from PCs severely affects cerebellum-dependent motor functions: both in mutant mice and in spinocerebellar ataxia type 6 patients, selective degeneration of PCs induce motor dysfunction (Frontali, 2001; Porras-Garcia et al., 2013), and PC-specific vesicular GABA transporter knockout mice exhibit motor impairment (Kayakabe et al., 2013).

We demonstrate that MAM-2201 inhibits neurotransmitter release at PF-PC, interneuron-PC, and CF-PC synapses in a concentration-dependent manner (Figs. 3–6), and reduces the number of spikelets in CF-evoked complex spikes (Fig. 7*A* and *B*). Assuming that, in humans, MAM-2201 inhibits neurotransmitter release at these synapses, the inhibition at PF-PC synapses could cause failure of simple spike generation in PCs. The inhibition of interneuron-PC synapses may weaken the feed-forward inhibition, leading to decreased precision of PC spike outputs. MAM-2201-induced reduction of spikelets in complex spikes (Fig. 7*A* and *B*) could cause a decrease in the number of action potentials that propagate to the synaptic terminals of PCs. Consequently, MAM-2201 may interrupt normal GABAergic inhibition onto the deep cerebellar nuclear neurons and vestibular nuclear neurons, and thus could affect cerebellum-dependent motor coordination. This speculation could be supported by the report that consumption of drugs of abuse containing analogs of MAM-2201 can cause cerebellar dysfunction such as disturbance of finger-to-finger test (Musshoff et al., 2014).

4.3. Possible effects of MAM-2201 on cerebellar LTD initiated by dendritic Ca^{2+} transients and on motor learning functions

PF-PC LTD is thought to underlie cerebellar motor learning in mammals (Yuzaki, 2012). This learning is impaired in transgenic mice that exhibit a deficit in the expression of LTD *in vitro* (Kakegawa et al., 2008). Induction of LTD requires association of PF and CF activation both *in vivo* and *in vitro* (Ito, 2001). At the cellular level, CF synaptic inputs to PCs evoke dendritic Ca^{2+} transients, which play crucial roles in the expression of LTD (Konnerth et al., 1992). Interestingly, Carey and Regehr reported that presynaptic inhibition of CF-PC synapses by noradrenaline alters the complex spike waveform and decreases CF-evoked dendritic Ca^{2+} transients, leading to interference with the induction of LTD (Carey and Regehr, 2009). This noradrenergic modulation shares many features with our observations of MAM-2201-induced changes of CF-evoked responses in PCs (Figs. 6 and 7): depression of CF-PC EPSCs via presynaptic mechanisms, reduction of the number of spikelets in complex spikes, and attenuation of CF-induced Ca^{2+} transients in PC dendrites. Taken together, MAM-2201 may interfere with the induction of LTD *in vitro* and might result in an impairment of cerebellar motor learning *in vivo*. Further work will be needed to clarify whether MAM-2201 indeed blocks the induction of LTD.

4.4. Implications for adverse effects of MAM-2201 on other brain functions

In the brain, CB1Rs are widely and abundantly expressed, and numerous *in vitro* studies have revealed that activation of CB1Rs by agonists suppresses synaptic transmission in several regions such as the hippocampus, nucleus accumbens, striatum, and cerebellar cortex (Kano et al., 2009). Moreover, in rat hippocampal slice preparations, pharmacological activation of CB1Rs modulates long-term potentiation in the CA1 region (Navakkode and Korte, 2014), and *in vivo* administration of WIN impairs hippocampal-dependent short-term memory (Hampson and Deadwyler, 2000). WIN also activates the "reward circuitry" in the brain, including the ventral tegmental area-nucleus accumbens pathway, and alters reward-

related behaviors in a similar manner to other reward-enhancing addictive drugs (Gardner, 2005). In this study, we demonstrated that MAM-2201 suppresses synaptic transmission in the cerebellum and that this action parallels that induced by WIN (Figs. 3–5). Taken together, in humans, MAM-2201 could cause psychoactive effects that are similar to those observed in the laboratory animal experiments using WIN or other synthetic cannabinoids.

Acknowledgments

This work was supported by Health Labour Sciences Research Grants. We thank Dr. Nobutake Hosoi (Gunma University) for technical advice on intracellular Ca^{2+} imaging.

References

Atwood, B.K., Huffman, J., Straiker, A., Mackie, K., 2010. JWH018, a common constituent of 'Spice' herbal blends, is a potent and efficacious cannabinoid CB receptor agonist. Br. J. Pharmacol. 160, 585–593.
Auwarter, V., Dresen, S., Weinmann, W., Muller, M., Putz, M., Ferreiros, N., 2009. 'Spice' and other herbal blends: harmless incense or cannabinoid designer drugs? J. Mass Spectrom. 44, 832–837.
Brown, S.P., Safo, P.K., Regehr, W.G., 2004. Endocannabinoids inhibit transmission at granule cell to Purkinje cell synapses by modulating three types of presynaptic calcium channels. J. Neurosci. 24, 5623–5631.
Bruno, A., Lembo, F., Novellino, E., Stornaiuolo, M., Marinelli, L., 2014. Beyond radiodisplacement techniques for identification of CB1 ligands: the first application of a fluorescence-quenching assay. Sci. Rep. 4, 3757.
Carey, M.R., Regehr, W.G., 2009. Noradrenergic control of associative synaptic plasticity by selective modulation of instructive signals. Neuron 62, 112–122.
Derungs, A., Schwaninger, A.E., Mansella, G., Bingisser, R., Kraemer, T., Liechti, M.E., 2013. Symptoms, toxicities, and analytical results for a patient after smoking herbs containing the novel synthetic cannabinoid MAM-2201. Forensic Toxicol. 31, 164–171.
DeSanty, K.P., Dar, M.S., 2001. Cannabinoid-induced motor incoordination through the cerebellar CB(1) receptor in mice. Pharmacol. Biochem. Behav. 69, 251–259.
Diana, M.A., Levenes, C., Mackie, K., Marty, A., 2002. Short-term retrograde inhibition of GABAergic synaptic currents in rat Purkinje cells is mediated by endogenous cannabinoids. J. Neurosci. 22, 200–208.
Dousmanis, A.G., Pennefather, P.S., 1992. Inwardly rectifying potassium conductances in AtT-20 clonal pituitary cells. Pflugers Arch. 422, 98–104.
Felder, C.C., Joyce, K.E., Briley, E.M., Glass, M., Mackie, K.P., Fahey, K.J., Cullinan, G.J., Hunden, D.C., Johnson, D.W., Chaney, M.O., Koppel, G.A., Brownstein, M., 1998. LY320135, a novel cannabinoid CB1 receptor antagonist, unmasks coupling of the CB1 receptor to stimulation of cAMP accumulation. J. Pharmacol. Exp. Ther. 284, 291–297.
Frontali, M., 2001. Spinocerebellar ataxia type 6: channelopathy or glutamine repeat disorder? Brain Res. Bull. 56, 227–231.
Gardner, E.L., 2005. Endocannabinoid signaling system and brain reward: emphasis on dopamine. Pharmacol. Biochem. Behav. 81, 263–284.
Hagiwara, S., Miyazaki, S., Rosenthal, N.P., 1976. Potassium current and the effect of cesium on this current during anomalous rectification of the egg cell membrane of a starfish. J. Gen. Physiol. 67, 621–638.
Hampson, R.E., Deadwyler, S.A., 2000. Cannabinoids reveal the necessity of hippocampal neural encoding for short-term memory in rats. J. Neurosci. 20, 8932–8942.
Hashimoto, K., Kano, M., 2013. Synapse elimination in the developing cerebellum. Cell. Mol. Life Sci. 70, 4667–4680.
Huestis, M.A., Gorelick, D.A., Heishman, S.J., Preston, K.L., Nelson, R.A., Moolchan, E.T., Frank, R.A., 2001. Blockade of effects of smoked marijuana by the CB1-selective cannabinoid receptor antagonist SR141716. Arch. Gen. Psychiatry 58, 322–328.
Irie, T., Fukui, I., Ohmori, H., 2006. Activation of GIRK channels by muscarinic receptors and group II metabotropic glutamate receptors suppresses Golgi cell activity in the cochlear nucleus of mice. J. Neurophysiol. 96, 2633–2644.
Irie, T., Matsuzaki, Y., Sekino, Y., Hirai, H., 2014. Kv3.3 channels harbouring a mutation of spinocerebellar ataxia type 13 alter excitability and induce cell death in cultured cerebellar Purkinje cells. J. Physiol. 592, 229–247.
Irie, T., Ohmori, H., 2008. Presynaptic GABA(B) receptors modulate synaptic facilitation and depression at distinct synapses in fusiform cells of mouse dorsal cochlear nucleus. Biochem. Biophys. Res. Commun. 367, 503–508.
Ito, M., 2001. Cerebellar long-term depression: characterization, signal transduction, and functional roles. Physiol. Rev. 81, 1143–1195.
Kakegawa, W., Miyazaki, T., Emi, K., Matsuda, K., Kohda, K., Motohashi, J., Mishina, M., Kawahara, S., Watanabe, M., Yuzaki, M., 2008. Differential regulation of synaptic plasticity and cerebellar motor learning by the C-terminal PDZ-binding motif of GluRdelta2. J. Neurosci. 28, 1460–1468.
Kano, M., Ohno-Shosaku, T., Hashimotodani, Y., Uchigashima, M., Watanabe, M., 2009. Endocannabinoid-mediated control of synaptic transmission. Physiol. Rev. 89, 309–380.
Kawamura, Y., Fukaya, M., Maejima, T., Yoshida, T., Miura, E., Watanabe, M., Ohno-Shosaku, T., Kano, M., 2006. The CB1 cannabinoid receptor is the major cannabinoid receptor at excitatory presynaptic sites in the hippocampus and cerebellum. J. Neurosci. 26, 2991–3001.
Kayakabe, M., Kakizaki, T., Kaneko, R., Sasaki, A., Nakazato, Y., Shibasaki, K., Ishizaki, Y., Saito, H., Suzuki, N., Furuya, N., Yanagawa, Y., 2013. Motor dysfunction in cerebellar Purkinje cell-specific vesicular GABA transporter knockout mice. Front. Cell. Neurosci. 7, 286.
Khaliq, Z.M., Raman, I.M., 2005. Axonal propagation of simple and complex spikes in cerebellar Purkinje neurons. J. Neurosci. 25, 454–463.
Kikura-Hanajiri, R., Uchiyama, N., Kawamura, M., Goda, Y., 2013. Changes in the prevalence of new psychoactive substances before and after the introduction of the generic scheduling of synthetic cannabinoids in Japan. Drug Test. Anal..
Konnerth, A., Dreessen, J., Augustine, G.J., 1992. Brief dendritic calcium signals initiate long-lasting synaptic depression in cerebellar Purkinje cells. Proc. Natl. Acad. Sci. U. S. A. 89, 7051–7055.
Korn, H., Faber, D.S., 1991. Quantal analysis and synaptic efficacy in the CNS. Trends Neurosci. 14, 439–445.
Kreitzer, A.C., Regehr, W.G., 2001. Retrograde inhibition of presynaptic calcium influx by endogenous cannabinoids at excitatory synapses onto Purkinje cells. Neuron 29, 717–727.
Kubo, Y., Reuveny, E., Slesinger, P.A., Jan, Y.N., Jan, L.Y., 1993. Primary structure and functional expression of a rat G-protein-coupled muscarinic potassium channel. Nature 364, 802–806.
Kushmerick, C., Price, G.D., Taschenberger, H., Puente, N., Renden, R., Wadiche, J.I., Duvoisin, R.M., Grandes, P., von Gersdorff, H., 2004. Retroinhibition of presynaptic Ca^{2+} currents by endocannabinoids released via postsynaptic mGluR activation at a calyx synapse. J. Neurosci. 24, 5955–5965.
Levenes, C., Daniel, H., Soubrie, P., Crepel, F., 1998. Cannabinoids decrease excitatory synaptic transmission and impair long-term depression in rat cerebellar Purkinje cells. J. Physiol. 510 (Pt 3), 867–879.
Llinas, R., Walton, K.D., Lang, E.J., 2004. Cerebellum. In: Shepard, G.M. (Ed.), The Synaptic Organization of the Brain, fifth ed. Oxford University Press, New York, NY, US, pp. 271–309.
Lonati, D., Buscaglia, E., Papa, P., Valli, A., Coccini, T., Giampreti, A., Petrolini, V.M., Vecchio, S., Serpelloni, G., Locatelli, C.A., 2014. MAM-2201 (analytically confirmed) intoxication after "synthacaine" consumption. Ann. Emerg. Med..
Luk, T., Jin, W., Zvonok, A., Lu, D., Lin, X.Z., Chavkin, C., Makriyannis, A., Mackie, K., 2004. Identification of a potent and highly efficacious, yet slowly desensitizing CB1 cannabinoid receptor agonist. Br. J. Pharmacol. 142, 495–500.
Mackie, K., 2008. Signaling via CNS cannabinoid receptors. Mol. Cell. Endocrinol. 286, S60–S65.
Mackie, K., Lai, Y., Westenbroek, R., Mitchell, R., 1995. Cannabinoids activate an inwardly rectifying potassium conductance and inhibit Q-type calcium currents in AtT20 cells transfected with rat brain cannabinoid receptor. J. Neurosci. 15, 6552–6561.
Maejima, T., Hashimoto, K., Yoshida, T., Aiba, A., Kano, M., 2001. Presynaptic inhibition caused by retrograde signal from metabotropic glutamate to cannabinoid receptors. Neuron 31, 463–475.
McKay, B.E., Turner, R.W., 2005. Physiological and morphological development of the rat cerebellar Purkinje cell. J. Physiol. 567, 829–850.
Mittmann, W., Koch, U., Hausser, M., 2005. Feed-forward inhibition shapes the spike output of cerebellar Purkinje cells. J. Physiol. 563, 369–378.
Monory, K., Blaudzun, H., Massa, F., Kaiser, N., Lemberger, T., Schutz, G., Wotjak, C.T., Lutz, B., Marsicano, G., 2007. Genetic dissection of behavioural and autonomic effects of Delta(9)-tetrahydrocannabinol in mice. PLoS Biol. 5, e269.
Moosmann, B., Kneisel, S., Girreser, U., Brecht, V., Westphal, F., Auwarter, V., 2012. Separation and structural characterization of the synthetic cannabinoids JWH-412 and 1-[(5-fluoropentyl)-1H-indol-3yl]-(4-methylnaphthalen-1-yl)methanone using GC-MS, NMR analysis and a flash chromatography system. Forensic Sci. Int. 220, e17–22.
Musshoff, F., Madea, B., Kernbach-Wighton, G., Bicker, W., Kneisel, S., Hutter, M., Auwarter, V., 2014. Driving under the influence of synthetic cannabinoids ("Spice"): a case series. Int. J. Legal Med. 128, 59–64.
Navakkode, S., Korte, M., 2014. Pharmacological activation of CB1 receptor modulates long term potentiation by interfering with protein synthesis. Neuropharmacology 79, 525–533.
Patel, S., Hillard, C.J., 2001. Cannabinoid CB(1) receptor agonists produce cerebellar dysfunction in mice. J. Pharmacol. Exp. Ther. 297, 629–637.
Porras-Garcia, M.E., Ruiz, R., Perez-Villegas, E.M., Armengol, J.A., 2013. Motor learning of mice lacking cerebellar Purkinje cells. Front. Neuroanat. 7, 4.
Regehr, W.G., Carey, M.R., Best, A.R., 2009. Activity-dependent regulation of synapses by retrograde messengers. Neuron 63, 154–170.
Safo, P.K., Cravatt, B.F., Regehr, W.G., 2006. Retrograde endocannabinoid signaling in the cerebellar cortex. Cerebellum 5, 134–145.
Safo, P.K., Regehr, W.G., 2005. Endocannabinoids control the induction of cerebellar LTD. Neuron 48, 647–659.
Saito, T., Namera, A., Miura, N., Ohta, S., Miyazaki, S., Osawa, M., Inokuchi, S., 2013. A fatal case of MAM-2201 poisoning. Forensic Toxicol. 31, 333–337.
Seely, K.A., Lapoint, J., Moran, J.H., Fattore, L., 2012. Spice drugs are more than harmless herbal blends: a review of the pharmacology and toxicology of synthetic cannabinoids. Prog. Neuro Psychopharmacol. Biol. Psychiatry 39, 234–243.

Shen, M., Thayer, S.A., 1999. Delta9-tetrahydrocannabinol acts as a partial agonist to modulate glutamatergic synaptic transmission between rat hippocampal neurons in culture. Mol. Pharmacol. 55, 8–13.
Showalter, V.M., Compton, D.R., Martin, B.R., Abood, M.E., 1996. Evaluation of binding in a transfected cell line expressing a peripheral cannabinoid receptor (CB2): identification of cannabinoid receptor subtype selective ligands. J. Pharmacol. Exp. Ther. 278, 989–999.
Shuvaev, A.N., Horiuchi, H., Seki, T., Goenawan, H., Irie, T., Iizuka, A., Sakai, N., Hirai, H., 2011. Mutant PKC{gamma} in spinocerebellar ataxia type 14 disrupts synapse elimination and long-term depression in Purkinje cells in vivo. J. Neurosci. 31, 14324–14334.
Szabo, B., Than, M., Thorn, D., Wallmichrath, I., 2004. Analysis of the effects of cannabinoids on synaptic transmission between basket and Purkinje cells in the cerebellar cortex of the rat. J. Pharmacol. Exp. Ther. 310, 915–925.
Takahashi, K.A., Linden, D.J., 2000. Cannabinoid receptor modulation of synapses received by cerebellar Purkinje cells. J. Neurophysiol. 83, 1167–1180.
Taura, F., Sirikantaramas, S., Shoyama, Y., Shoyama, Y., Morimoto, S., 2007. Phytocannabinoids in Cannabis sativa: recent studies on biosynthetic enzymes. Chem. Biodivers. 4, 1649–1663.
Uchiyama, N., Kawamura, M., Kikura-Hanajiri, R., Goda, Y., 2013. URB-754: a new class of designer drug and 12 synthetic cannabinoids detected in illegal products. Forensic Sci. Int. 227, 21–32.
Vardakou, I., Pistos, C., Spiliopoulou, C., 2010. Spice drugs as a new trend: mode of action, identification and legislation. Toxicol. Lett. 197, 157–162.
Vincent, P., Marty, A., 1996. Fluctuations of inhibitory postsynaptic currents in Purkinje cells from rat cerebellar slices. J. Physiol. 494 (Pt 1), 183–199.
Voogd, J., Glickstein, M., 1998. The anatomy of the cerebellum. Trends Cogn. Sci. 2, 307–313.
Wilson, R.I., Nicoll, R.A., 2002. Endocannabinoid signaling in the brain. Science 296, 678–682.
Xu-Friedman, M.A., Regehr, W.G., 1999. Presynaptic strontium dynamics and synaptic transmission. Biophys. J. 76, 2029–2042.
Yuzaki, M., 2012. Cerebellar LTD vs. motor learning-lessons learned from studying GluD2. Neural Netw..
Zheng, N., Raman, I.M., 2010. Synaptic inhibition, excitation, and plasticity in neurons of the cerebellar nuclei. Cerebellum 9, 56–66.
Zucker, R.S., Regehr, W.G., 2002. Short-term synaptic plasticity. Annu Rev. Physiol. 64, 355–405.

正常機能

ミクログリアの発生と分化

佐藤　薫

ミクログリアの発生と分化過程

脳の免疫機能担当細胞として長らく知られてきたミクログリアは脳細胞の5%を占める．Macrophage 1 antigen (Mac1)，major histocompatibility complex (MHC) class Ⅱ，CD68，F4/80やfragment，crystallizable(Fc)受容体，low density lipoprotein(LDL)受容体といった細胞表面抗原を発現していること，貪食能，サイトカイン分泌といった機能を有することなど，モノサイトやマクロファージに類似点が多いため，脳内炎症レベルの決定細胞として長らく炎症を伴う病態研究の対象となってきた．ミクログリアをモノサイトやマクロファージと決定的に区別できる細胞表面抗原がまだ見つかっていないため，その起源についてもモノサイトやマクロファージと共通であると長らく考えられてきた．しかし2010～12年にかけて，ミクログリアが系統的に発生過程の早い時期にマクロファージと分かれていることが明らかにされた．ミクログリアは胎生7.5日齢に骨髄前駆細胞から分化し胎生8.5～9.5日齢にはすでに脳内に移行している[1,2]．Ginhouxらは，造血幹細胞(モノサイトやマクロファージのもとになる幹細胞)の完成前である胎生7日齢に，ミクログリア前駆細胞がすでに卵黄嚢で発生しており，胎生9日齢までにこれらの細胞が脳に移行してミクログリアとなることを実験的に証明した[1]．これは神経幹細胞であるラジアルグリアが脳内に発生する(胎生10.5日齢)よりも早いタイミングの出来事である．このミクログリア前駆細胞はCsf1受容体を発現したMyb(－)，PU.1依存的であることも[2]，Myb(＋)な造血幹細胞とは異なる点である．一方，病態時には血液脳関門のバリア機能低下により血球系細胞の脳内浸潤が起こるが，これらの細胞がミクログリアにはならないことも示されている．モノサイトやマクロファージのみがgreen fluorescent protein(GFP)標識されたマウスに実験的脳脊髄炎(experimental allergic encephalomyelitis：EAE)を発症させると，EAE症状の重篤度に応じてモノサイトが脊髄に浸潤するが，炎症終息後にGFP陽性細胞は消失した[3]．以上のことから，脳内で生理的な機能を持つミクログリアのほとんどが胎生7.5日齢に脳内に移行したミクログリア前駆細胞の子孫たちであると考えられる．ところが，このように共通の先祖を持ちながらミクログリアは中枢神経系の発達，機能分化とともに，ミエリン，血管系，血液脳関門，周囲細胞の細胞外マトリックス，神経伝達物質，といった周囲環境との相互作用によって，その領域，その時期に特異的な形態，抗原発現パターン，増殖パターン，生理機能を獲得する[4,5]．さらに言えば，一領域中のミクログリア集団の中に感染や外傷に対して非常に劇的に反応する集団とそうでもない集団が含まれていることもあり[6]，ミクログリアと微細な周囲環境との相互作用が起こっていると考えられる．

ミクログリアは，正常脳でよくみられるような，細かく発達した多くの突起を持つ「静止型」と神経炎症等の病変部に集積しているアメボイド状の「活性化型」との間を環境の変化に応じて行き来する細胞である．しかし最近の研究で，静止型ミクログリアはその発達した突起により周囲環境を実に積極的に探索していることが明らかとなっている[5]．したがって「静止型」，「活性化型」はもはや言葉通りに捉えきれなくなっている．現在，ミクログリアの活性状態はM0，M1，M2ステージというカテゴリーで表現されるが，この概念はそもそもマクロファージ研究から導入された[7]．マクロファージは外部刺激に対する反応によってM1，M2a，M2b，M2cというカテゴリーに分けられるが[8]，ミクログリアと異なる点は，分類に有効な35種類の表面抗原が明らかになっている点である．M1ミクログリアは炎症誘発特性，M2ミクログリアが抗炎症特性を持つ，と言われるが，そのどちらにも入らないM0ミクログリアという集団も発見されている[4]．M1，M2の中間とも言えるミクログリアも存在する．生後初期マウスのミクログリアはM1遺伝子(iNOS，TNFα)とM2遺伝子(Arginase-1)の両者を高発現している．M0，M1，M2ステージの他に

さとう かおる　国立医薬品食品衛生研究所薬理部第一室長(中枢神経薬理)

0289-0585/20/¥90/頁/JCOPY

HoxB8というホメオボックスタンパク質の発現によってミクログリアを分類しているグループもいる[9]．HoxB8(+)細胞はCD11b(+)ミクログリアの15%を占め，卵黄嚢から分化するミクログリアとは異なる細胞集団であると報告されている．HoxB8を欠損したマウスは強迫性障害スペクトラムに伴う脱毛症と非常によく似た症状が現れるため，病態解明への応用が期待されている．

脳室下帯ミクログリアに関する最近の知見

脳室帯(ventricular zone：VZ)と脳室下帯(subventricular zone：SVZ)は一生を通じて神経新生やグリア新生が起こる領域であることが明らかとなって久しい．主要な投射神経は胎生期に，アストロサイトは胎生期から生後初期まで，オリゴデンドロサイトは胎生後期から生後初期にかけて，介在神経は胎生後期以降新生される[10]．一方，上で述べたように胎生8.5〜9.5日齢にはアメボイド型のミクログリアが脳内にすでに存在している[1,2]．ミクログリアは生後初期に爆発的に増加するが[11]，発達が進むにつれアメボイド型のミクログリアは減少し成体においてほとんど静止型になる[12]．しかし，胎生期の神経新生にミクログリアがどのように関わっているかについては2013年にCunninghamらが報告するまで，ほとんどわかっていなかった[13]．彼らは胎生期の大脳皮質神経細胞新生過程の後半において，ミクログリアが貪食作用によって神経前駆細胞プールの細胞数を調節していることを明らかにした．このとき，ミクログリアが貪食した細胞はアポトーシスを起こしていない点は興味深い．成体海馬歯状回顆粒細胞層(subgranular zone：SGZ)での神経新生の場合，ミクログリアはアポトーシスを起こした細胞を貪食しているからである[14]．発達期SVZと成体SGZでの神経新生とミクログリアの関連について，さらなる解明が待たれる．

生後SVZの神経新生におけるミクログリアの役割については胎生期に増してほとんど情報がなかったが，2006年に，SVZのように神経新生が活発な領域とそれ以外の領域とでミクログリアの活性化や機能に差があることが指摘された[15]．最近われわれは，生後初期に活性化型ミクログリアがSVZに一過的に集積しており，成熟に伴い，より突起の発達したミクログリアが白質まで分散するようになることを見出した．われわれは生後初期SVZでこのように特異な挙動を示すミクログリアが，SVZにおける神経新生およびオリゴデンドロサイト新生を促進することを明らかにした[16](図1)．SVZは一生を通じて神経新生が継続するものの，年を重ねるにつれ新生細胞数は激減する．われわれのデータでも，生後30日齢のSVZに活性化型ミクログリアはすでにほとんど存在せず，SVZ神経新生動態と相関がある．興味深いことに，SVZでの神経新生に対するミクログリアの作用はSVZ中の位置によって異なるようである．われわれも体軸の中間あたり，線条体と海馬が対面するあたりが最もミクログリア密度が高いことを見出している．この細胞分布の偏りは血管系が関与している可能性がある．血管は成体脳SVZにおいて神経新生ニッチとなることが知られているが[17,18]，SVZは血管叢と呼ばれるほど血管が発達しており[19,20]，特にSVZ中心部は腹側から大きな血管が来ている[20,21]．血管から多種の液性因子が放出されていることはよく知られているが[17]，大脳皮質にミクログリアが移行するのに重要なシグナルカスケードであるCXCL12/CXCR4シグナル[22]の関与などが考えられる．成体脳における脳室上衣下層(subependymal zone：SEZ)では吻側尾側方向，背側腹側方向に高度に領域化されており，各領域からは異なる神経細胞系列が新生してくることも知られている[23]．また，背側SEZではより多くのオリゴデンドロサイト新生が起こることも知られている[24]．今後，SVZ領域をさらに細分化してミクログリアの役割について検討する必要があろう．

成体脳SVZからとってきた神経幹細胞や神経前駆細胞の場合，Th2ヘルパーT細胞由来サイトカインによって刺激されたミクログリアが神経新生やオリゴデンドロサイト新生を促進する[25]．このとき，ミクログリアから放出されるIGF-1が作用に関与していることが示唆されている．しかし，生後初期SVZにおいてはIGF-1を発現しているミクログリアはわずかに確認されるが，IGF-1はミクログリアの神経新生促進作用の作用本体ではなかった[16]．われわれは，ミクログリアが神経新生，オリゴデンドロサイト新生を促進するメカニズムとして生後4〜9日齢のSVZにおいて一過的に濃度が上昇するサイトカイン群(IL-1β, IL-6, TNFα, IFNγ)が重要であることを明らかとした．興味深いのは，神経幹細胞塊(neurosphere)とミクログリアの共培養系を用いた実験で，上記4種のサイトカインのう

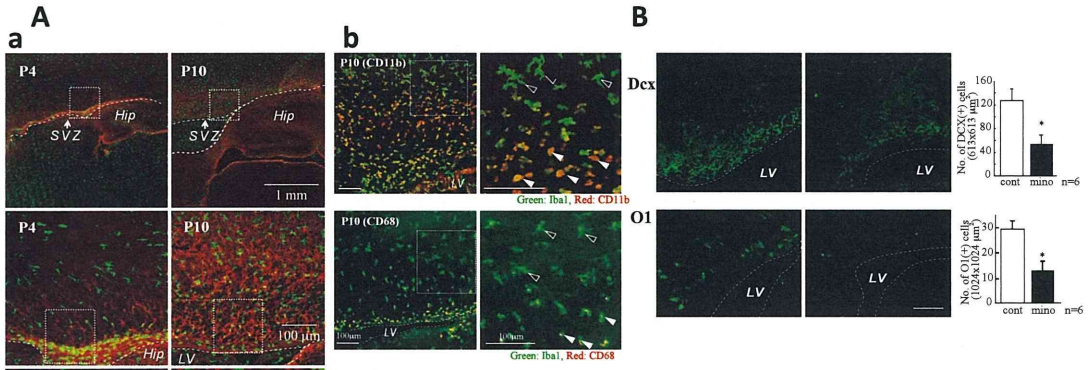

図 1　生後初期 SVZ ミクログリアの神経新生およびオリゴデンドロサイト新生における役割

A-a）生後初期 SVZ に活性化型ミクログリアが集積していることを見出した．

A-b）集積ミクログリアの活性化型マーカー（CD11b，CD68）の発現．白矢頭は Iba1（＋）marker（＋）細胞を表す．

B）ミノサイクリンを P1-4 で腹腔内投与すると，神経前駆細胞マーカー Dcx とオリゴデンドロサイト前駆細胞マーカー O1 を発現する細胞数が有意に減少した．*p＜0.05 vs. control group, student's *t* test（N＝6）．（Shigemoto-Mogami ら[16]より改変）

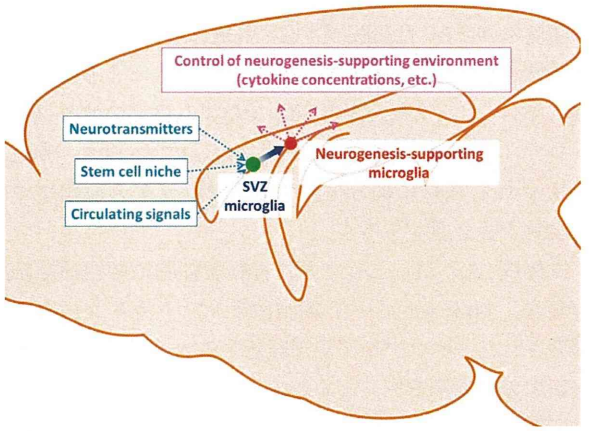

図 2

SVZ ミクログリアは脳内・脳外環境からの信号に応じてサイトカイン環境を調節する‘Hub’として機能しているのではないか．

ち 1 種のサイトカイン機能を機能中和抗体で阻害してもミクログリアの作用に何ら影響はなかったが，全てのサイトカインを同時に阻害するとミクログリアの作用が消失したことである．この結果は神経新生やオリゴデンドロサイト新生を複数のサイトカインが相補的に促進していることを示唆している．これまで，神経新生に関するサイトカインの作用としては，神経前駆細胞が IL-1β，IL-1R1，IL-1R2 を発現し，IL-1β は神経前駆細胞の増殖と分化を調節していること[26]，IL-6 が IL-6R を介して神経新生を促進すること[27]などが報告されていたが，複数サイトカインによる相補的な作用は報告がなかった．Li らは IFNγ の作用はミクログリア存在下では表現系が異なることを示しており，われわれが示した相補的作用を支持するものである[28]．そもそも，IL-1β，IL-6，TNFα，IFNγ は炎症性サイトカインとして，LPS（lipopolysaccharide）刺激[29]，EAE[30]，status epilepticus（SE）[31]といった病理的条件下では神経新生を抑制する本体として研究されてきた．しかし，より穏やかな実験条件では異なる作用が発揮される．炎症モデル作成のために使われる LPS は，適用条件（適用時間など）をわずかに調整することでミクログリアの神経新生への影響が変化する[32]．サイトカイン自身も濃度によって作用が変化する．TNFα は 1 ng/mL では神経幹細胞を増殖する一方，10 ng/mL 以上の濃度でアポトーシスを起こす[33]．われわれのデータでは，ミノサイクリンがミクログリアの活性化を抑制すると，神経前駆細胞の数は半分以下に減少するのに対し，それぞれのサイトカインレベルの減少は皆一様に穏やかであった．サイトカインはミクログリアだけでなく

アストロサイトなどの周囲細胞からも放出される．おそらく，ミクログリアからのサイトカイン放出が‘cytokine storm’[34]には遠く及ばない程度の，‘cytokine drizzling’とも言える連続的なサイトカイン放出トリガーとなっていることが予想される．

むすび

われわれにとって次の課題は，生後初期ミクログリアの活性化機構の解明である．重大なヒントとして胎生期から生後にかけてSVZでのミクログリア機能が大きく変化する点があげられる．体内を循環している種々のメディエーターは誕生の前後で質，量ともに大きく変化する[35]．われわれは，SVZミクログリアはこのような脳内・脳外環境からの信号に応じてサイトカイン環境を調節する‘Hub’として機能しているのではないかと考えている(図2)．このような脳外から脳内への情報デリバリー，それに伴うミクログリアによる神経新生の調節メカニズムの解明は，発達障害を含む神経障害治療にもブレークスルーをもたらすことが期待される．

文献

1) Ginhoux F, Greter M, Leboeuf M, et al. Fate mapping analysis reveals that adult microglia derive from primitive macrophages. Science. 2010；330：841-5.
2) Schulz C, Gomez Perdiguero E, Chorro L, et al. A lineage of myeloid cells independent of Myb and hematopoietic stem cells. Science. 2012；336：86-90.
3) Ajami B, Bennett JL, Krieger C, et al. Infiltrating monocytes trigger EAE progression, but do not contribute to the resident microglia pool. Nat Neurosci. 2011；14：1142-9.
4) Butovsky O, Jedrychowski MP, Moore CS, et al. Identification of a unique TGF-β-dependent molecular and functional signature in microglia. Nat Neurosci. 2014；17：131-43.
5) Kettenmann H, Hanisch UK, Noda M, Verkhratsky A. Physiology of microglia. Physiol Rev. 2011；91：461-553.
6) Scheffel J, Regen T, Van Rossum D, et al. Toll-like receptor activation reveals developmental reorganization and unmasks responder subsets of microglia. Glia. 2012；60：1930-43.
7) Sica A, Mantovani A. Macrophage plasticity and polarization：in vivo veritas. J Clin Invest. 2012；122：787-95.
8) Geissmann F, Gordon S, Hume DA, et al. Unravelling mononuclear phagocyte heterogeneity. Nat Rev Immunol. 2010；10：453-60.
9) Chen SK, Tvrdik P, Peden E, et al. Hematopoietic origin of pathological grooming in Hoxb8 mutant mice. Cell. 2010；141：775-85.
10) Wang DD, Bordey A. The astrocyte odyssey. Prog Neurobiol. 2008；86：342-67.
11) Sminia T, de Groot CJ, Dijkstra CD, et al. Macrophages in the central nervous system of the rat. Immunobiology. 1987；174：43-50.
12) Zusso M, Methot L, Lo R, et al. Regulation of postnatal forebrain amoeboid microglial cell proliferation and development by the transcription factor Runx1. J Neurosci. 2012；32：11285-98.
13) Cunningham CL, Martínez-Cerdeño V, Noctor SC. Microglia regulate the number of neural precursor cells in the developing cerebral cortex. J Neurosci. 2013；33：4216-33.
14) Sierra A, Encinas JM, Deudero JJ, et al. Microglia shape adult hippocampal neurogenesis through apoptosis-coupled phagocytosis. Cell Stem Cell. 2010；7：483-95.
15) Goings GE, Kozlowski DA, Szele FG. Differential activation of microglia in neurogenic versus non-neurogenic regions of the forebrain. Glia. 2006；54：329-42.
16) Shigemoto-Mogami Y, Hoshikawa K, Goldman JE, et al. Microglia enhance neurogenesis and oligodendrogenesis in the early postnatal subventricular zone. J Neurosci. 2014；34：2231-43.
17) Goldberg JS, Hirschi KK. Diverse roles of the vasculature within the neural stem cell niche. Regen Med. 2009；4：879-97.
18) Quaegebeur A, Lange C, Carmeliet P. The neurovascular link in health and disease：molecular mechanisms and therapeutic implications. Neuron. 2011；71：406-24.
19) Ihrie RA, Alvarez-Buylla A. Lake-front property：a unique germinal niche by the lateral ventricles of the adult brain. Neuron. 2011；70：674-86.
20) Shen Q, Wang Y, Kokovay E, et al. Adult SVZ stem cells lie in a vascular niche：a quantitative analysis of niche cell-cell interactions. Cell Stem Cell. 2008；3：289-300.
21) Dorr A, Sled JG, Kabani N. Three-dimensional cerebral vasculature of the CBA mouse brain：a magnetic resonance imaging and micro computed tomography study. Neuroimage. 2007；35：1409-23.
22) Arnò B, Grassivaro F, Rossi C, et al. Neural progenitor cells orchestrate microglia migration and positioning into the developing cortex. Nat Commun. 2014；5：5611.
23) Merkle FT, Mirzadeh Z, Alvarez-Buylla A. Mosaic organization of neural stem cells in the adult brain. Science. 2007；317：381-4.
24) Ortega F, Gascon S, Masserdotti G, et al. Oligodendrogliogenic and neurogenic adult subependymal zone neural stem cells constitute distinct lineages and exhibit differential responsiveness to Wnt signalling. Nat Cell Biol. 2013；15：602-13.
25) Butovsky O, Ziv Y, Schwartz A, et al. Microglia activated by IL-4 or IFN-gamma differentially induce neurogenesis and oligodendrogenesis from adult stem/progenitor cells. Mol Cell Neurosci. 2006；31：149-60.
26) Wang X, Fu S, Wang Y, et al. Interleukin-1beta mediates proliferation and differentiation of multipotent neural precursor cells through the activation of SAPK/JNK pathway. Mol Cell Neurosci. 2007；36：343-54.
27) Islam O, Gong X, Rose-John S, Heese K. Interleukin-6 and neural stem cells：more than gliogenesis. Mol Biol Cell. 2009；20：188-99.
28) Li L, Walker TL, Zhang Y, et al. Endogenous interferon gamma directly regulates neural precursors in the non-inflammatory brain. J Neurosci. 2010；30：9038-50.
29) Monje ML, Toda H, Palmer TD. Inflammatory blockade restores adult hippocampal neurogenesis. Science. 2003；302：1760-5.
30) Ben-Hur T, Ben-Menachem O, Furer V, et al. Effects of proinflammatory cytokines on the growth, fate, and motility of multipotential neural precursor cells. Mol Cell Neurosci. 2003；24：623-31.
31) Iosif RE, Ekdahl CT, Ahlenius H, et al. Tumor necrosis factor receptor 1 is a negative regulator of progenitor proliferation in adult hippocampal neurogenesis. J Neurosci. 2006；26：9703-12.
32) Cacci E, Ajmone-Cat MA, Anelli T, et al. In vitro neuronal and glial differentiation from embryonic or adult neural precursor cells are differently affected by chronic or acute activation of microglia. Glia. 2008；56：412-25.
33) Bernardino L, Agasse F, Silva B, et al. Tumor necrosis factor-alpha modulates survival, proliferation, and neuronal differentiation in neonatal subventricular zone cell cultures. Stem Cells. 2008；26：2361-71.
34) Clark IA. The advent of the cytokine storm. Immunol Cell Biol. 2007；85：271-3.
35) Spencer SJ, Mouihate A, Galic MA, Pittman QJ. Central and peripheral neuroimmune responses：hyporesponsiveness during pregnancy. J Physiol. 2008；586：399-406.

Sensors and Materials, Vol. 27, No. 10 (2015) 1035–1044
MYU Tokyo

S & M 1140

Improvements in Enzyme-Linked Photoassay Systems for Spatiotemporal Observation of Neurotransmitter Release

Kazunori Watanabe, Nobuto Takahashi, Naohiro Hozumi[1] and Sachiko Yoshida*

Department of Environmental and Life Sciences,
Toyohashi University of Technology, 1-1 Hibarigaoka, Tempaku-cho, Toyohashi 441-8580, Japan
[1]Int'l Cooperation Center for Engineering Education Development/
Department of Electrical & Electronic Information Engineering,
Toyohashi University of Technology, 1-1 Hibarigaoka, Tempaku-cho, Toyohashi 441-8580, Japan

(Received February 23, 2015; accepted September 25, 2015)

Key words: neurotransmitter, glutamate, GABA, enzyme immobilization, UV LED

Neurotransmitters and neuronal releasing molecules are not only the regulators of neuronal function but also the indicators of neuronal conditions. Glutamate and γ-amino butyric acid (GABA) play important roles in cerebellar differentiation and function. In the mature cortex, they are released from synapses and taken up by transporter molecules. We have developed enzyme-linked photoassay systems for glutamate, GABA, and adenosine triphosphate (ATP), and reported their release in the developing cerebellar cortex. Our systems showed slow transmitter release in the immature cerebellum, whereas it was hard to detect the fast synaptic release from mature neurons, because there were some limitations in time resolution and data depth derived from a charge-coupled device (CCD), and the enzyme-linked photodevice was sometimes unstable. In this study, we report the dynamic observation of neurotransmitter release in the developing cerebellar slices using improved photodevices and a high-speed 16-bit CCD. With this new system, the rapid measurement of transmitter release in a young-adult cerebellar cortex is possible. We suggest that these photoassay systems are useful for observing synaptic release in several diseases.

1. Introduction

Neurotransmitter molecules released from neurons are not only the regulators of neuronal transduction but also the indicators of neuronal conditions.[1–3] Glutamate and γ-aminobutyric acid (GABA) are known as typical transmitters in the brain's cortex, and they play important roles as stimulators and suppressors, respectively. Lack of balance in the release of glutamate and GABA may lead to autism, epilepsy, or Parkinson's disease.[4]

*Corresponding author: e-mail: syoshida@ens.tut.ac.jp

ISSN 0914-4935

To observe spatiotemporal neurotransmitter release in the cerebellar cortex, we have recently developed an enzyme-linked photoassay system, which is a device with an immobilized enzyme on a quartz glass surface. Using this system, we observed glutamate or GABA release in developing cerebellar slices using either new or authorized methods.[5] Enzyme-linked photoassay is sensitive and selective, and it can discriminate the substrates from their pharmacological analogues. Our system can detect transmitter release in the cerebral cortex,[6] hippocampus, retina, and cultured cells,[7] and made it possible to detect the release of adenosine triphosphate (ATP),[8] glucose, sucrose, and fructose. On the other hand, enzymes tend to denature and separate from the quartz. For the detection of transmitter release in mature neuronal circuits, increasing the sensitivity and stability of the device is required.

In this paper, we propose new immobilizing methods and discuss the optimization of the enzyme-linked photoassay.

2. Materials and Methods

2.1 *Substrate and enzyme reaction*

Imaging neurotransmitter release was monitored for the reaction in which oxidoreductases generate reduced nicotinamide adenine dinucleotide (NAD^+) or diphosphonucleotide ($NADP^+$). For glutamate, GABA, or adenosine triphosphate (ATP) imaging, we used glutamate dehydrogenase, GABA disassembly enzyme [GABase, Fig. 1(a)] or glyceraldehyde 3-phosphate dehydrogenase, respectively.[9–11] The NADH or NADPH, the reductants of NAD^+ or $NADP^+$, respectively, which is generated stoichiometrically, emits 480 nm fluorescence after excitation at 340–365 nm.

2.2 *Surface photoexcitation*

For UV excitation, a quartz glass plate illuminated with an ultraviolet light-emitting diode (UV-LED, Nichia, Tokushima, Japan) was used. Leaking UV light onto the glass surface excited fluorescent NADH or NADPH [Fig. 1(b)].

2.3 *Imaging apparatus*

All fluorescence images through the inverted microscope (IX73, Olympus Co., Ltd., Tokyo, Japan) were observed by a cooled charge-coupled device (CCD) (ORCA-ER CCD) or a high-speed complimentary metal-oxide semiconductor (CMOS) (ORCA-Flash 4.0) camera, supplied by Hamamatsu Photonics Co., Ltd., Hamamatsu, Japan. Imaging data were analyzed by iVision software (BD Biosciences, San Jose, CA, USA).

2.4 *Enzyme immobilization and sample preparation*

Enzymes were typically covalently immobilized on the quartz glass surface using a silane coupling agent and a crosslinking agent, 3-aminopropyltriethoxy silane (3-APTS) and glutaraldehyde, respectively [Fig. 2(a)].[12] These surface modifications determine both the stability of the enzyme reaction and the distance between the sample and the glass surface.

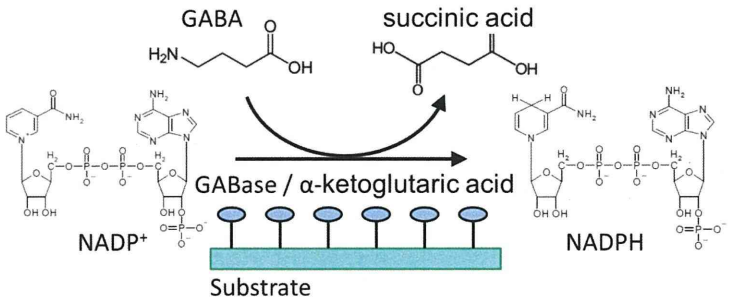

(a)

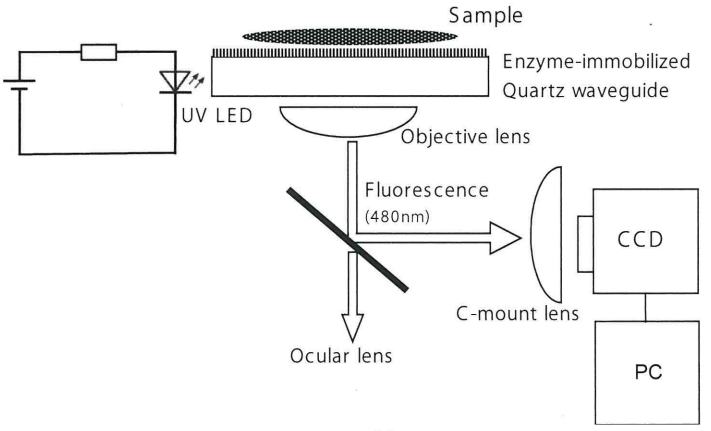

(b)

Fig. 1. (Color online) (a) Released neurotransmitters are oxidized by the oxidoreductase, and NAD(P)H is formed stoichiometrically. In GABA oxidization, released GABA is converted to succinic acid with NADPH formation by GABase. (b) Schematic diagram of the enzyme-linked photoassay system. The oxidoreductases are immobilized on the quartz glass surface, and the excitation light radiating from UV-LED passes through the quartz waveguide. Fluorescent images are obtained by CCD or CMOS, and analyzed using a computer system.

In some cases, glass surfaces were treated with either aromatic crosslinkers, 1,4-phenylene diisothiocyanate (1,4-DIC), or 1,3-phenylene diisothiocyanate [1,3-DIC, Fig. 2(b)], and glutaraldehyde (GA).[13] Others were treated with a phosphonic acid, 11-aminoundecylphosphonic acid [11-AUPA, Fig. 2(c)], as a replacement for 3-APTS.[14]

Cerebellar acute slices were treated from postnatal day 3 (P3) to P15 in rats, sliced sagittally to a thickness of 400 μm with a rotor slicer (Dohan EM, Kyoto, Japan),

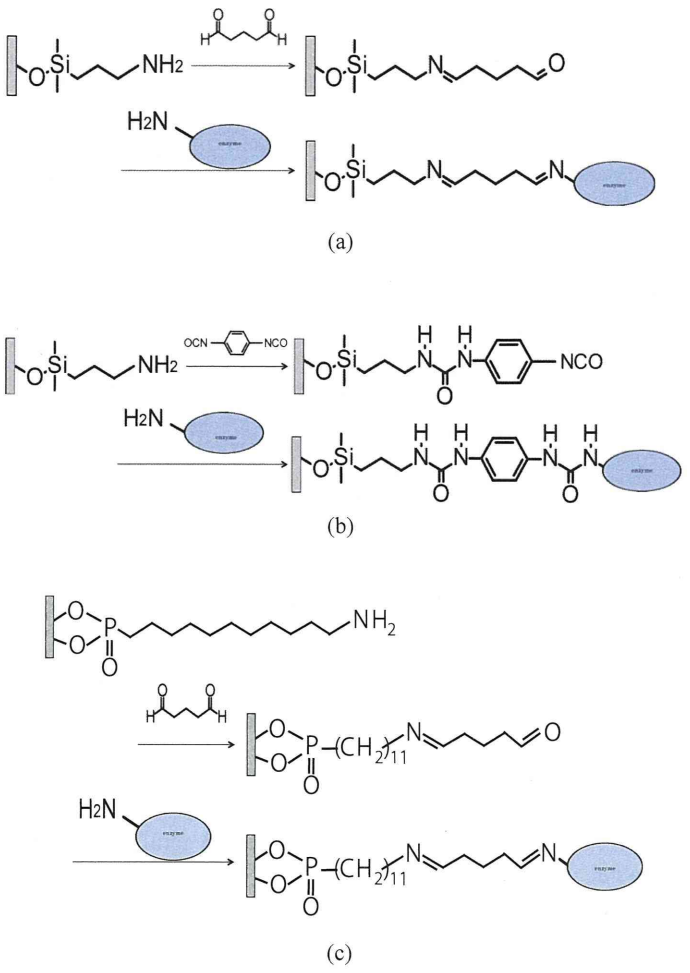

Fig. 2. (Color online) (a) Method of enzyme immobilization using 3-APTS and glutaraldehyde. Surface treatment and crosslinking between waveguide quartz and enzyme. (b) Crosslinking using 1,3-DIC. (c) Surface treatment with 11-AUPA.

and incubated in oxygen-aerated PBS for 45 min. All experimental procedures were approved by the committee for the use of animals at Toyohashi University of Technology and by the guidelines of the Ministry of Education, Culture, Sports, Science and Technology, Japan.

3. Results

3.1 *Spatiotemporal observation of glutamate release*

Figure 3(a) shows an illustration of rat cerebellar development. In the developing cerebellum, neuronal arrangement and circuit formation progress after birth. Granule cells, small input neurons, proliferate and migrate down from the external granular layer (EGL) to the internal granular layer (IGL). Purkinje cells, major output neurons, develop their dendrites and associate neuronal connections between granule cells and other interneurons. The layer of Purkinje cell somas is identified to be the Purkinje layer (PL). A neuronal circuit layer forms the molecular layer (ML).[15,16] To understand the roles of neurotransmitters in the cerebellar development, we have developed a new visualizing device and, with it, we have observed spatiotemporal molecular dynamics.

Using the enzyme-linked photoassay system, we have observed many kinds of transmitter release in several developmental stages and organs. Our system has visualized both spontaneous and responsive transmitter release processes with 0.5 s time resolution. Figures 3(b)–3(k) show the transitions in glutamate release in response to 100 μM GABA application in developing cerebellar slices.[17] Glutamate was released in both the EGL and the IGL, whereas the PL was indicated by a negative line. In the developing cerebellum, the granule cells that distributed in the EGL and IGL are the only neurons that release glutamate, so both layers showed fluorescence activities. Glutamate release in P3 cerebellar slices appeared in both layers slowly but continuously, whereas it started rapidly in the lower EGL and then spread to the IGL within a short time in P7 celebellar slices.[18] Granule cells in the P3 cerebellum did not develop sufficiently to react to GABA stimulation nor release the transmitter actively, but they still proliferated. On the other hand, the granule cells in the P7 cerebellum developed sufficiently to react to GABA stimulation, so they released glutamate rapidly.

Although spatiotemporal observation could give us dynamic information about neuronal reaction, our system needs to be improved in terms of stability, sensitivity and time resolution for us to observe fast synaptic transmissions. The targets of our improvements were the (1) sensing CCD, (2) excitation waveguide, and (3) manner of enzyme immobilization shown in Fig. 2.

3.2 *Effects of new crosslinkers and surface treatment*

Two types of glass devices with either aromatic crosslinkers, 1,3-DIC or 1,4-DIC, and GA were examined to observe spontaneous GABA release with 500 ms time resolution using ORCA ER CCD. The device formed using 1,3-DIC and GA gave images with a better contrast of GABA release than the GA crosslinked device in the P10 cerebellar slice [Fig. 4(a)], whereas it showed no difference in the P6 cerebellar slice. The 1,4-DIC crosslinked device yielded no good images.

The aromatic crosslinkers make the glass surface hydrophobic. Because mature brain tissues become hydrophobic as the myelin structure develops, 1,3-DIC crosslinking should increase the affinity of the enzyme for the tissues.

The binding between the glass and the acceptor molecules has been weak, because the silane coupling agents tend to undergo hydrolysis under biological conditions. The

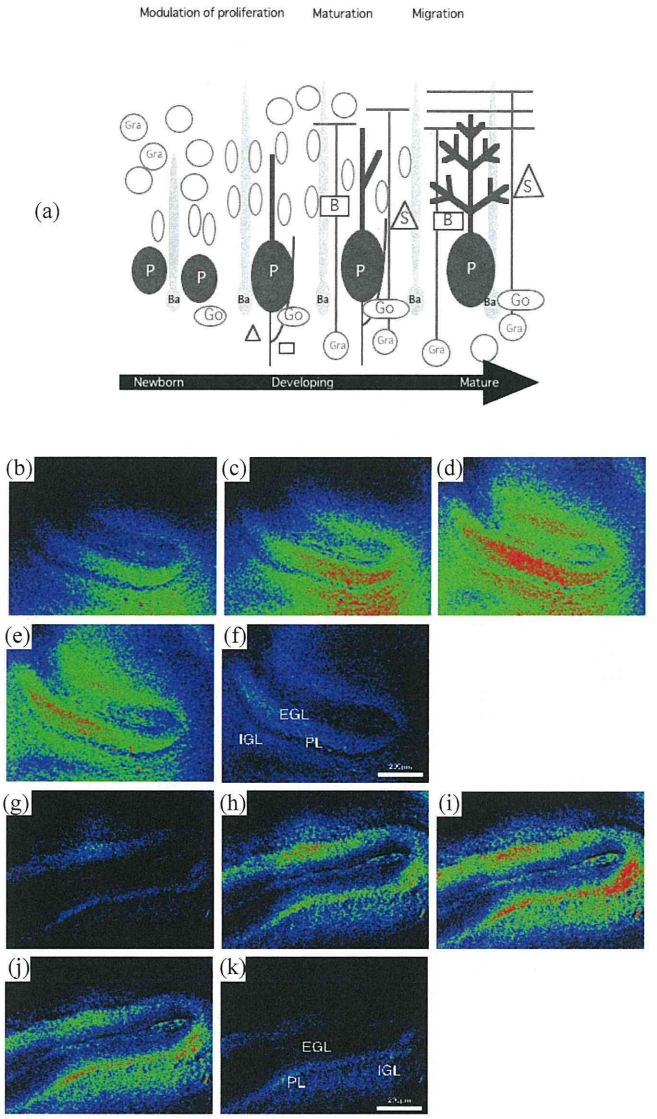

Fig. 3. (a) Diagram of cerebellar development. In the newborn cerebellum (1 to 3 days after birth), granule cell progenitors (Gra) proliferate in the EGL, while immature Purkinje cells (P) form the PL with Golgi cells (Go) and some Bergmann glia (Ba). During the developement, 5 to 7 days after birth, Gra-cells elongate their axon and migrate inside, and P-cells spread their dendrites and connect to other neurons within two weeks. B denotes basket cells, and S, satellite cells. Evoked glutamate wave with GABA application in developing cerebellar cortex. (b)–(f): 2.0, 4.5, 7.0, 12.5, and 23.5 s after stimulation in P3 cerebellar cortex, respectively. (g)–(k): 0.5, 2.5, 4.0, 11.0, and 16.0 s after stimulation in P7 cerebellar cortex, respectively.

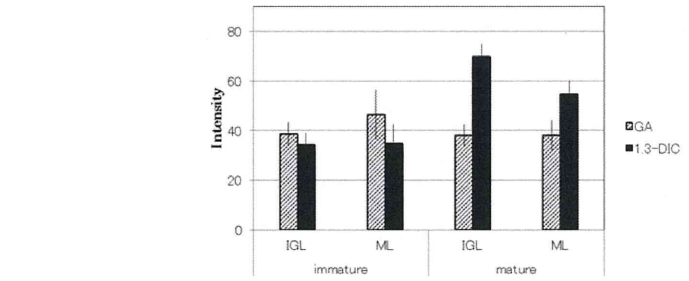

(a)

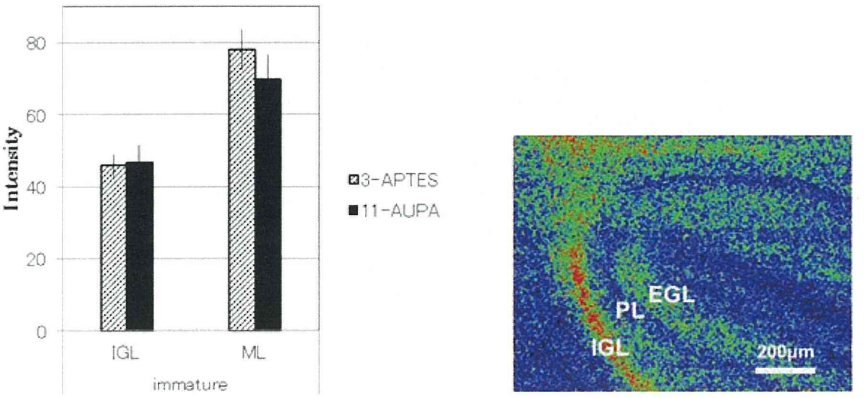

(b) (c)

Fig. 4. (Color online) (a) New crosslinker, 1,3-DIC, gave us better contrast images than GA in mature cerebellar observation, while it made little difference from GA in immature organ. (b) The 11-AUPA-GA treatment showed the same result as the APTS-GA treatment in the immature organ. (c) Spontaneous GABA release image in P12 cerebellar slice using 1,3-DIC crosslinking glass device.

surface treatment by 11-AUPA, as a replacement for 3-APTS, was expected to inhibit hydrolysis, but it had low affinity for the glass. We constituted a new glass device with 11-AUPA-coupling enzymes and examined its sensitivity and stability. Figure 4(b) shows that the new device performed with the same sensitivity and stability as the device with APTS.

3.3 *Observation using high-speed CMOS camera*

The fluorescence intensity of NADH is very low and is only a few thousands of the intensity of typical artificial fluorescence. To collect data with sufficient time resolution, a highly sensitive and rapid data transferring camera is required. The time resolution

shown in Fig. 3 is 0.5 s for the 12-bit ORCA CCD, which is too low to detect the synaptic transmitter reaction.

A 16-bit CMOS camera, Flash 4.0, could detect weak light and transfer data in less than a microsecond. Using this camera, transient glutamate release could be detected with a 20 ms time resolution (Fig. 5). In developing the P7 cerebellum, glutamate release was increased in the EGL by applying a glutamate receptor-stimulating agent, α-amino-3-hydroxy-5-methyl-4-isoxazolepropionic acid (AMPA). Even in the premature P14 cerebellum, the increment in the rate of glutamate release was observed. It was not strong and noiseless, but the AMPA stimulation-induced glutamate release was observed in the ML and IGL where the glutamatergic neurons are distributed.

4. Discussion

The detection of neurotransmitter release gives us important information about developmental conditions and diseases. Parkinson's disease, a degenerative disorder of the central nervous system, is caused by the alteration of the release of neurotransmitters. The detection of the spatial or temporal alteration of the release would require early diagnosis and treatment of Parkinson's disease. In immature or lesioned neuronal organs, transmitters are released and taken up slowly, so the time resolution required is from 0.5 to 1 s. In young-adult stages, the release speed becomes higher than that in the immature stage within 20 ms.

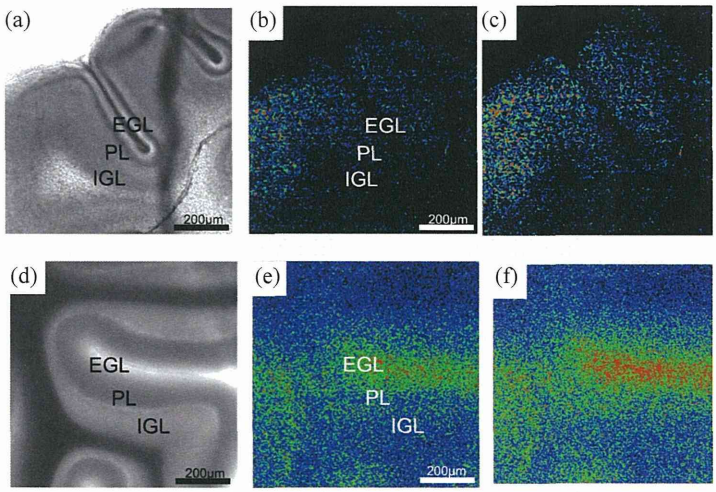

Fig. 5 (Color online) Evoked glutamate release images to AMPA stimulation for 20 ms time resolution using Flash 4.0 CMOS system. (a)–(c) P7 cerebellar slice; (d)–(f) P14 cerebellar slice. (a) and (d) Phase contrast light images. (b) and (e) Fluorescence images before stimulation and (c) and (f) just after AMPA stimulation.

Enzyme-linked assays were applied previously for chemical detection because of their specificity. In spatial observations, however, their fluorescence intensity is too weak to detect. Our enzyme-linked photodevice was developed to detect spatiotemporal neurotransmitter release, and it was improved to observe rapid synaptic release. New crosslinkers could contribute to a more sensitive detection, and the phosphonic surface treatment would expand the range of applications. In order to detect a high-speed transmitter release, both the light accumulation system for weak fluorescence and the close contact between the specimen and the enzyme are required. At present, our photodetection system detects several ms releases from neuronal synapses in the presence of noise, and in the future, it could give us more noiseless observations using an optimal image processing system.

5. Conclusions

The newly developed enzyme-linked photoassay is useful for the visualization of neurotransmitter release in brain slices. In the immature cerebellum, the granule cells release glutamate slowly or rapidly at their stage of neuronal development and synaptogenesis.

Using a fast new system, the rapid measurement of transmitter release in a young-adult cerebellar cortex became possible. Crosslinkers and other device techniques are required for stable observations. We suggest that the photoassay systems have advantages for the observation of synaptic release in several diseases.

Acknowledgements

This study was supported by grants from Scientific Research (C) 23500516 and 26350498, and Health Labor Sciences Research.

References

1 J. Moran and M. Rivera-Gaxiola: J. Neurosci. Res. **33** (1992) 239.
2 P. Varju, Z. Katarova, E. Madarasz and G. Szabo: Cell Tissue Res. **305** (2001) 239.
3 D. Casel, J. Brockhaus and J. W. Deitmer: J. Physiol. **568** (2005) 111.
4 M. Ochi, S. Shiozaki and H. Kase: Neuroscience **127** (2004) 223.
5 T. Morishima, M. Uematsu, T. Furukawa, Y. Yanagawa, A. Fukuda and S. Yoshida: Neurosci. Res. **67** (2010) 347.
6 T. Wang, T. Kumada, T. Morishima, S. Iwata, T. Kaneko, Y. Yanagawa, S. Yoshida and A. Fukuda: Cereb Cortex **24** (2014) 1088.
7 S. Yoshida and N. Hozumi: JNNS **20** (2013) 14.
8 H. Muramoto, Y. Sekino, N. Hozumi, A. Fukuda and S. Yoshida: 42th Neuroscience Meeting (2012) (CD-ROM).
9 B. Innocenti, V. Parpura and P. G. Haydon: J. Neurosci. **20** (2000) 1800.
10 M. Israel and B. Lesbats: J. Neurochem. **67** (1996) 2624.
11 S. Yoshida: Japanese Patent No. 4480952 (2010).
12 L. Blasi, L. Longo, PP. Pompa, L. Manna, G. Ciccarella, G. Vasapollo, R. Cingolani, R. Rinaldi, A. Rizzello, R. Acierno, C. Storelli and M. Maffia: Biosens. Bioelectron. **21** (2005) 30.